

SHORT-TERM VARIABILITY OF X-RAYS FROM ACCRETING NEUTRON STAR VELA X-1: II.
MONTE-CARLO MODELINGHIROKAZU ODAKA¹, DMITRY KHANGULYAN¹, YASUYUKI T. TANAKA², SHIN WATANABE¹,
TADAYUKI TAKAHASHI^{1,3}, AND KAZUO MAKISHIMA^{3,4}

ABSTRACT

We develop a Monte Carlo Comptonization model for the X-ray spectrum of accretion-powered pulsars. Simple, spherical, thermal Comptonization models give harder spectra for higher optical depth, while the observational data from Vela X-1 show that the spectra are harder at higher luminosity. This suggests a physical interpretation where the optical depth of the accreting plasma increases with mass accretion rate. We develop a detailed Monte-Carlo model of the accretion flow, including the effects of the strong magnetic field ($\sim 10^{12}$ G) both in geometrically constraining the flow into an accretion column, and in reducing the cross section. We treat bulk-motion Comptonization of the infalling material as well as thermal Comptonization. These model spectra can match the observed broad-band *Suzaku* data from Vela X-1 over a wide range of mass accretion rates. The model can also explain the so-called “low state”, in which the luminosity decreases by an order of magnitude. Here, thermal Comptonization should be negligible, so the spectrum instead is dominated by bulk-motion Comptonization.

Subject headings: radiation mechanisms: general, accretion, stars: neutron, pulsars: individual (Vela X-1), X-rays: binaries

1. INTRODUCTION

Binary systems harboring a massive star and a black hole (or a neutron star) form the population of the brightest X-ray sources. In these sources emission is powered by accretion from the optical companion onto the compact object, and is typically dominated by the thermal emission from the accretion disk. However, this is not the case when the compact object is a strongly magnetized neutron star (i.e., a pulsar). The key difference between this and the conventional scenario is related to the disruption of the accretion flow by the pulsar magnetic field. The structure of the disrupted flow is governed by the magnetic field, which re-directs the accreted plasma towards the magnetic poles of the pulsar. This results in the formation of a so-called *accretion column* (see, e.g., Becker & Wolff 2005, and references therein). The physical conditions realized in the accretion column differ significantly from ones typically formed in accretion disks. Therefore, accreting binary pulsars represent a subclass of bright X-ray sources with rather specific properties. Given the complexity of the processes taking place in the accretion column, a proper interpretation of observational data obtained in the X-ray energy band requires a detailed modeling of an entire range of different physical processes.

Conservation of energy implies that the **luminosity** is roughly determined by the accretion rate. However, the spectral shape does not allow any simple interpretation.

Therefore, studying of the spectral properties might shed light on the physical conditions of the accretion flow in binary pulsars. Vela X-1 is the brightest wind-fed accreting pulsar and displays strong time variability in the X-ray band (e.g. Kreykenbohm et al. 2008), therefore this object provides us with an ideal laboratory for studying the physical conditions of the accreted plasma. In order to obtain information regarding spectral features of the emission produced by the accretion flow in Vela X-1, we analyzed X-ray data collected with *Suzaku* (Odaka et al. 2013, hereafter Paper I). The observation was 145 ks long and has an exposure time of 100 ks. Owing to the wide-band coverage and the high signal-to-noise performance of instruments onboard *Suzaku* (Mitsuda et al. 2007; Takahashi et al. 2007; Kokubun et al. 2007), we extracted 56 sequential X-ray spectra of Vela X-1 for short time intervals of 2 ks in an energy range from 2.5 keV to 50 keV. These spectra sample a wide luminosity range, allowing us to constrain the physical parameters of the accretion flow.

As it was shown in Paper I, the X-ray spectra obtained with *Suzaku* from Vela X-1 are the best fitted by the “NPEX” model (a combination of negative and positive power laws with an exponential cutoff by a common folding energy; Mihara 1995; Makishima et al. 1999), i.e., by

$$\frac{dN}{dE} = (A_1 E^{-\Gamma} + A_2 E^2) \exp\left(-\frac{E}{E_f}\right), \quad (1)$$

where A_1 , A_2 , $\Gamma > 0$ and E_f are parameters used for fitting. However, the relation of these parameters to the physical properties of the emitter is vague and, obviously, can vary with a specific physical scenario. This ambiguity is simply a reflection of the complexity of radiation mechanisms operating in these sources.

In this work, we attempt to link the physical properties of the flow to its observational manifestation as seen in the X-ray energy band from Vela X-1 (obtained in

¹ Institute of Space and Astronautical Science (ISAS), Japan Aerospace Exploration Agency (JAXA), 3-1-1 Yoshinodai, Chuo, Sagamihara, Kanagawa, 252-5210, Japan

² Hiroshima Astrophysical Science Center, Hiroshima University, 1-3-1 Kagamiyama, Higashi-Hiroshima, Hiroshima 739-8526, Japan

³ Department of Physics, University of Tokyo, 7-3-1 Hongo, Bunkyo, Tokyo, 113-0033, Japan

⁴ The Institute of Physical and Chemical Research, 2-1 Hirosawa, Wako, Saitama, 351-0198, Japan

Paper I). We consider Comptonization to be the dominant process for X-ray production. To account for a few key processes, in particular, for the geometry of accretion column, we exploited the Monte-Carlo approach. The paper is organized as follows: in Section 2 we present a description of the structure of the accretion flow together with simple analytical estimates, in Section 3 we present results of computations of pure thermal Comptonization, in Section 4 we report results obtained for the assumed structure of an accretion column. Finally, in Section 5 we discuss our results and in Section 6 we present our conclusions.

2. ACCRETION FLOW IN Vela X-1

For the conditions expected in Vela X-1, the optical star likely does not fill its Roche lobe. Therefore, the compact object can only accrete stellar matter via direct wind accretion. In a simple picture of this wind-fed accretion, the accretion flow is described by an analytical solution (Bondi & Hoyle 1944), which allows a straightforward interpretation: a small fraction of the wind material (wind passing within the so-called accretion radius of the compact object) is directly captured by the compact star's gravity, whereas the wind outside the radius escapes. Since the gravitational energy of the accreted matter is converted into X-ray radiation, this approach allows us to obtain an estimate of the X-ray luminosity L_X of the source:

$$L_X = \frac{(GM_*)^3 \dot{M}_{\text{wind}}}{R_* v_{\text{wind}}^4 D^2} \sim 10^{36} \text{ erg s}^{-1}, \quad (2)$$

where $R_* \sim 10$ km, $v_{\text{wind}} \sim 1000$ km s $^{-1}$, $M_* \sim 1.9M_\odot$, $\dot{M}_{\text{wind}} \sim 10^{-6}M_\odot\text{yr}^{-1}$ and $D \sim 50R_\odot$ are the radius of the accreting neutron star; the relative velocity of the wind seen from the accretion center; the mass of the compact star; the mass-loss rate of the donor star by the stellar wind; and the distance of the compact object from the center of the companion (donor) star, respectively (the values used for normalization of Equation (2) are similar to those expected in Vela X-1, see Watanabe et al. 2006, and references therein). Despite large uncertainties, Equation (2) provides a good estimate for typical X-ray luminosity of Vela X-1.

In contrast to the total luminosity, the emission spectral shape is not constrained from the first principles and is strongly influenced by the dominant radiation process, conditions of the accreted plasma and geometry of the flow. In the case of accretion onto a magnetized neutron star, the presence of the magnetic field should strongly influence all these properties. Indeed, close to the neutron star the magnetic field rapidly increases as $B = \mu/R^3$ (here $\mu = B_* R_*^3 \sim 10^{30}$ G cm 3 ; B_* denotes the magnetic field at the stellar surface), and for conditions expected in a wind-fed binary pulsar, the magnetic pressure should exceed the accretion flow ram pressure at certain distance, R_M (known as Alfvén radius). Accounting for the typical values of the relevant parameters and given the relatively weak dependence on them, the Alfvén radius is expected to be two or three orders of magnitude larger than the size of the neutron star (see e.g. Frank et al. 2002, §6.5). Thus, in the conventional scenario, the strong magnetic field of the neutron star disrupts the accretion flow at R_M , and then channels it

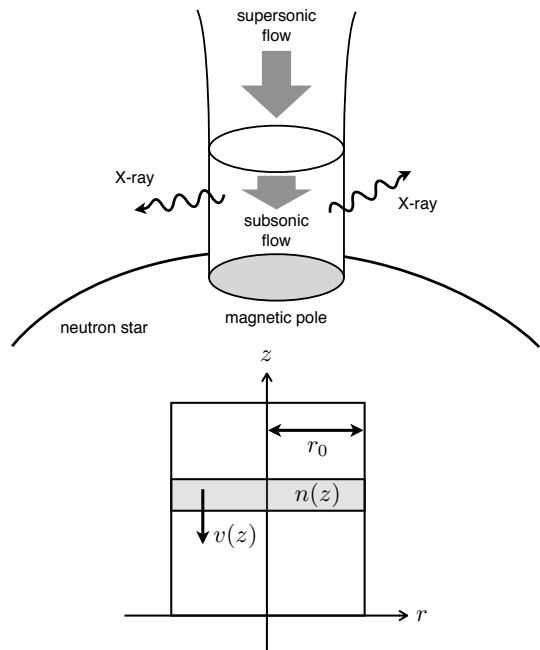


FIG. 1.— Schematic picture of an accretion column on a neutron star (upper panel); and sketch of its structure adopted for numerical modeling (bottom panel).

along the field lines to magnetic poles on the neutron star (Basko & Sunyaev 1976). The flow forms a column-like structure, which is called accretion column, as shown in Figure 1.

It is obvious that the flow moving at free-fall velocity, $v_{\text{ff}} = \sqrt{2GM_*/R_*} \sim 0.5c$, cannot be accreted by the neutron star. So, the flow is to be decelerated, and the excess of energy should be radiated through some mechanism. Thus, the dominant emission component should be formed in this compact region with quite specific physical properties. However, currently there is no self-consistent theory, which explains the dynamical and radiative properties of the accretion column. Such a theory should address the extreme complexity of nonlinear physical processes when the gas dynamics is completely coupled to both strong magnetic and strong radiation fields.

For high-luminosity X-ray pulsars, which are characterized by luminosities of $\sim 10^{38}$ erg s $^{-1}$, the above scenario was shown to be quite feasible (see, e.g., Becker 1998). Indeed, the radiation pressure in such systems is strong enough to form a radiation-dominated shock, which decelerates the accretion flow. While the in-falling gas passes through the shock, the kinetic energy is converted into X-rays and escapes from the accretion column. The critical luminosity for formation of a radiation-dominated shock is

$$L_{\text{crit}} = 3 \times 10^{37} \left(\frac{r_0}{R_*} \right) \left(\frac{M_*}{M_\odot} \right) \text{ erg s}^{-1}, \quad (3)$$

where r_0 denotes the radius of the accretion column (Basko & Sunyaev 1976; Becker 1998). Though wind-fed pulsars, such as Vela X-1, have relatively low luminosities $L_X \sim 10^{36}$ erg s $^{-1}$ due to smaller accretion rates, it is likely that they also possess radiation-dominated shocks close to the neutron star surfaces (White et al.

1983; Becker & Wolff 2007).

In what follows we adopted a one-dimensional model of the flow in the accretion column (Becker & Wolff 2007), i.e., all the plasma characteristics depend on only one coordinate: distance to the surface of neutron star (z coordinate), and the magnetic field is assumed to have only z -component (see Figure 1). In this model, the flow is decelerated by radiation-dominated shock near the surface, and the velocity profile derived by Becker (1998) can be written as

$$v(z) = -v_{\text{ff}} \left[1 - \left(\frac{7}{3} \right)^{-z/z_{\text{sp}}} \right]. \quad (4)$$

Here, v_{ff} denotes the free-fall velocity, and the sonic point z_{sp} , at which the velocity of the accretion flow becomes equal to a speed of sound, are given by

$$z_{\text{sp}} = \frac{r_0}{2\sqrt{3}} \left(\frac{\sigma_{\perp}}{\sigma_{\parallel}} \right)^{1/2} \ln \frac{7}{3} = 0.245 r_0 \left(\frac{\sigma_{\perp}}{\sigma_{\parallel}} \right)^{1/2}, \quad (5)$$

where $\sigma_{\parallel/\perp}$ are energy-averaged scattering cross sections for photons propagating parallel and perpendicular to the magnetic field, respectively. We can also obtain the number density of the plasma as a function of z by mass conservation (see Equation 9). In the case of the radiation-dominated shock, the velocity and density profiles are continuous unlike “normal” gas-dominated shocks, which have a discontinuous transition at the sonic point.

3. THERMAL COMPTONIZATION IN SPHERICAL MODEL

Although the fast bulk motion and the strong magnetic field affect the X-ray radiation from the accretion column, it is worthwhile to consider a simple, spherical model without magnetic fields and bulk motions prior to investigating more realistic but more complicated columnar flow models in Section 4. We therefore first examine the observed spectral shapes of Vela X-1 in a framework of a pure thermal Comptonization model. Using the Monte Carlo framework MONACO (Odaka et al. 2011), we performed simulations of spherical uniform Comptonizing clouds with different radial optical thicknesses. Based on this simple approach we estimate characteristic, effective parameters of the accretion plasma in the X-ray emitter.

3.1. Comptonization Spectrum

A Comptonization spectrum mainly depends on three characteristics of the source: the spectrum of the seed photons, the energy distribution of the Comptonizing electrons, and the optical depth. Since the X-ray cutoff energy provides a rough estimate of the electron temperature kT , the spectral shape revealed in Paper I (see § 4.2) indicates that the plasma temperature should be close to $kT \sim 7\text{keV}$. We therefore consider two cases for temperature, $kT = 6\text{ keV}$, 10 keV , in the simulations. The electron temperature also allows a natural definition of the spectrum of the seed photons. Namely, the energy spectrum of the seed photons has been assumed to be thermal bremsstrahlung from a plasma with the same temperature as the Comptonizing electrons. More specifically, the photon number distribution of the seed

photons is

$$\begin{aligned} N^{\text{ff}}(E) &= \frac{dn}{dV dt dE} = \frac{\varepsilon_{\nu}^{\text{ff}}}{hE} \\ &= 3.0 \times 10^{-15} \left(\frac{E}{1\text{ keV}} \right)^{-1} \left(\frac{kT}{1\text{ keV}} \right)^{-1/2} \\ &\quad \times Z^2 n_e n_i e^{-E/kT} \bar{g}_{\text{ff}} \text{ photons cm}^{-3} \text{ s}^{-1} \text{ keV}^{-1}, \end{aligned} \quad (6)$$

where $\varepsilon_{\nu}^{\text{ff}}$ is the energy emissivity of thermal bremsstrahlung; n_e and n_i are number densities of electrons and ions, and \bar{g}_{ff} is a velocity-averaged Gaunt factor (Rybicki & Lightman 1979).

In the numerical computations described in this section we assumed that the source of the seed photons is located in the center of electron cloud. This setup of the photon source is not the case of a realistic thermal, Comptonizing plasma, in which seed photons can be generated anywhere via bremsstrahlung by the plasma itself. However, we put the source at the center in order to characterize the thermal Compton spectrum by the optical depth seen by a photon traveling from the center toward the surface of the cloud. This characteristic value can be regarded as an “effective” optical depth that indicates a degree of thermal Comptonization.

The calculation was conducted for different Thomson thicknesses from the cloud center to the cloud surface in a range between 1 and 20. These model calculations allow us to relate the phenomenological parameters in the NPEX model to the physical characteristics of the emitting system. In Figure 2, we show spectra of thermal Comptonization for selected values, $\tau = 1, 8$ and 16 , of the optical depth. The simulation results are fitted to the NPEX model (Eq. 1) in the energy range of 2.5–60 keV. Though we are now interested in the spectral shape only, the normalizations of the spectra are determined by the required luminosity of the seed photons of $L = 1 \times 10^{36} \text{ erg s}^{-1}$ in a range of 0.1–100 keV at the distance of 1.9 kpc. The fitting results show that thermal Comptonization spectra are perfectly characterized by the NPEX model.

Figure 3 shows the fitted model parameters as functions of the optical thickness τ . Importantly, the photon index of the negative power law becomes hard with the optical thickness, being independent of the electron temperature in the considered range. Thus, the photon index Γ can be used as a good indicator of the optical thickness:

$$\tau = 14 - 1.85\Gamma. \quad (7)$$

The cutoff energy E_f is comparable to the electron temperature, but also changes with the optical thickness. The normalizations of the two power-law components have opposite dependence on the optical thickness, showing an approach to the saturation of the thermal Comptonization. However, since these normalization coefficients scale with the total flux and depend on the spectral slope, their absolute values are not suitable for spectral characterization.

Since the spectral slope weakly depends on physical properties except for the optical thickness, we propose that the ratio A_2/A_1 can also be used to indicate the degree of Comptonization, or the optical thickness of the

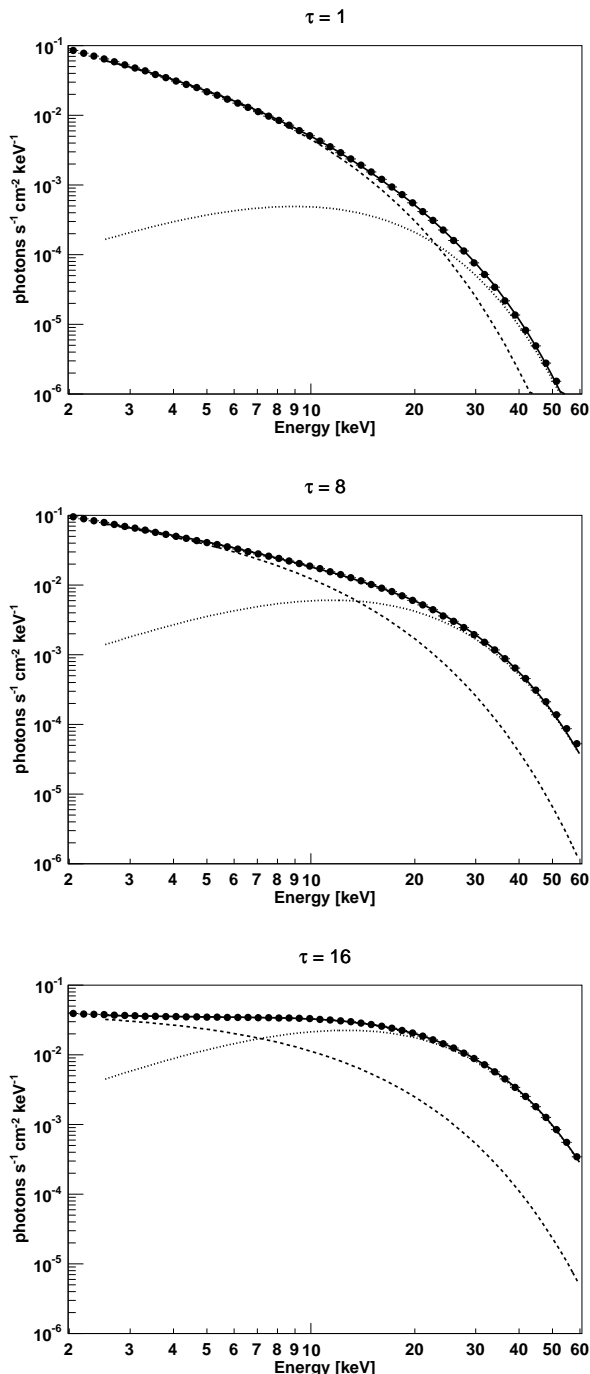


FIG. 2.— Examples of simulation spectral models of thermal Comptonization. These models assume a common electron temperature $kT = 6$ keV and different radial optical thicknesses $\tau = 1, 8, 16$ (as indicated at the top of each panel). Fitted NPEX models (solid), the negative (dashed) and the positive (dotted) power-law components are superposed. Statistical errors due to Monte Carlo sampling are sufficiently small compared with the filled circles showing the simulation data points.

Comptonizing cloud. To confirm it, we show the relation between A_2/A_1 and the optical thickness τ in the left panel of Figure 4. The ratio A_2/A_1 has strong dependence on the optical thickness with a relatively small difference due to the electron temperature, and moreover it can be regarded as a monotonically increasing function

of the optical thickness. In addition, it is helpful to see the relation between A_2/A_1 and the photon index Γ of the negative power-law component, which is also a good indicator of τ , as shown in the right panel of Figure 4. The normalization ratio A_2/A_1 significantly increases as the spectrum becomes hard. If thermal Comptonization plays an important role in generating X-ray radiation in an astrophysical object that shows spectral variability, such a remarkable correlation between A_2/A_1 and the spectral index, both of which can be directly determined by observation, should appear.

3.2. Comparison with Observations

Based on the simulation results presented in the previous section, we conclude that thermal Comptonization model implies a correlation between the power-laws' normalization ratio A_2/A_1 and the photon index Γ of the NPEX model. Since in Paper I we reported time dependent spectral properties of Vela X-1 obtained with *Suzaku* (the entire observation period of 145 ks was resolved over short periods of 2 ks), it is possible to test the inferred correlation against this set of observational data. In Figure 5, we show a comparison between the model prediction and the data. It can be seen that the correlation nicely agrees with the theoretical model shown in the right panel of Figure 4. We note that two exceptional points which show a very soft index $\Gamma \sim 1.7$ at a low-state (ID: 17 in Paper I) and a very hard index $\Gamma \sim -0.2$ at a sharp flaring (ID: 48 in Paper I) were removed from the plot.

While the positive power-law normalization A_2 is mathematically coupled with the photon index Γ , the large change of A_2/A_1 ranging over two orders of magnitude is consistent with changing the optical depth of the Comptonizing cloud. This result, therefore, suggests that thermal Comptonization can play an important role in generating the X-ray spectrum from Vela X-1.

As shown in Figure 6, the data suggest a phenomenological correlation between the photon index and X-ray luminosity, which can be converted into a relation between some key parameters describing the conditions in the accretion flow. Namely, the source luminosity is directly related to the mass accretion rate \dot{M} ($L \simeq GM_*\dot{M}/R_*$) and the photon index is linked to the production region opacity by Equation (7). Therefore, we obtain a relation between the accretion rate \dot{M} and the effective optical thickness τ of the accretion plasma, as shown in Figure 7. Within the context of the NPEX model the accretion rate and the optical thickness have a positive correlation. A linear function to describe the relation is

$$\tau = 4.3 \times \frac{\dot{M}}{10^{16} \text{ g s}^{-1}}. \quad (8)$$

Although, the disagreement between the observational points and the simple relation Equation (8) indicates a possible impact of other physical processes, the general tendency of the correlation of the optical depth and accretion rate supports the scenario of Comptonized X-ray radiation.

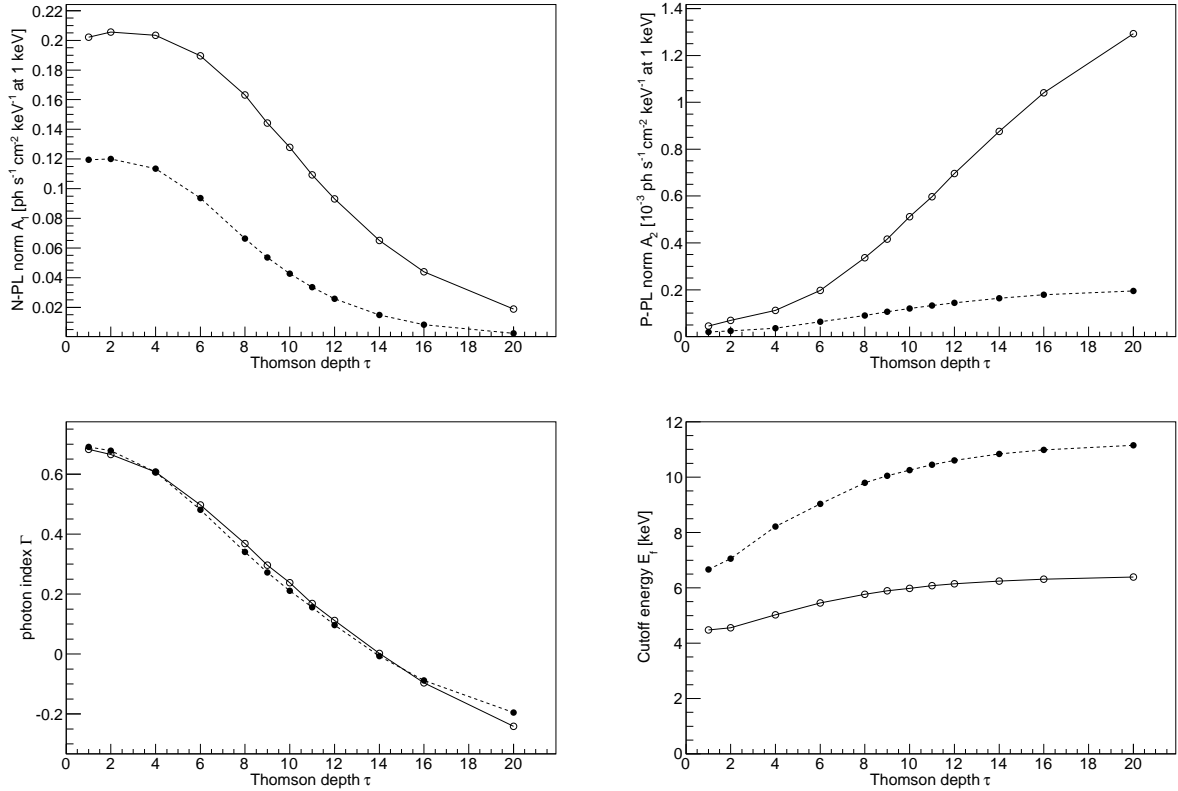


FIG. 3.— Fitted NPEX model parameters, the negative power-law (N-PL) normalization A_1 (top-left), the positive power-law (P-PL) normalization A_2 (top-right), the photon index Γ of the negative power law (bottom-left), and the cutoff energy E_f (bottom-right), as functions of the optical thickness τ of the clouds. The solid line with open circles and the dashed line with filled circles are the functions for $kT = 6$ keV and $kT = 10$ keV, respectively.

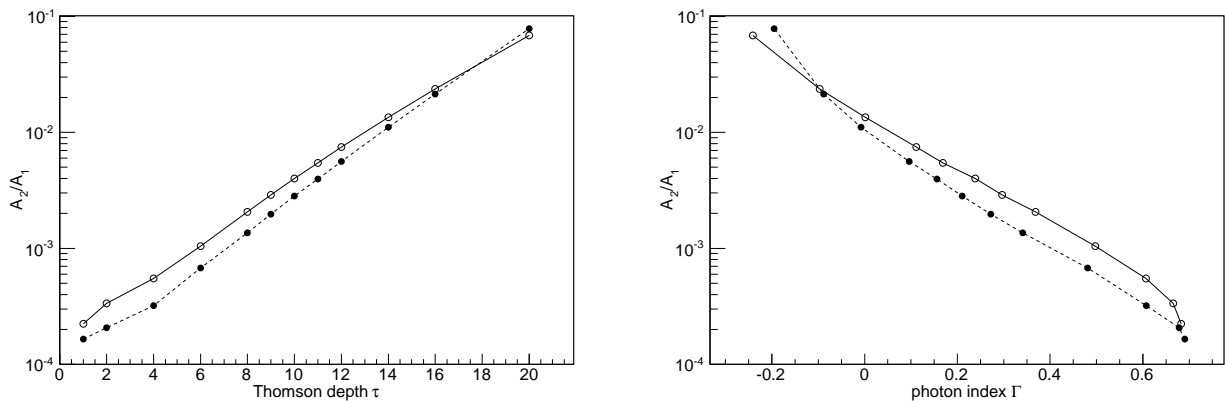


FIG. 4.— Left: ratio A_2/A_1 between the normalizations of two power-law components of the NPEX model as a function of the optical thickness τ . Right: relation between A_2/A_1 and the photon index Γ of the negative power-law component. The solid line with open circles and the dashed line with filled circles are the functions for $kT = 6$ keV and $kT = 10$ keV, respectively.

The pure thermal Comptonization model described in the previous section lacks geometrical and dynamical structure of the column and does not account for the impact of the magnetic field. Since these factors can introduce differences to the simple picture considered above, a physical model of the accretion column requires a more detailed treatment. In this section, we describe a self-consistent physical model of an accretion column on a

neutron star based on thermal and bulk Comptonization.

Before proceeding to a more detailed calculation, however, it is possible to obtain first order approximation to the structure of the column based on the results obtained in Section 3. Namely, assuming a simple geometry of the accretion column with a radius of r_0 in which the number density $n(z)$ and the bulk velocity $v(z)$ of the plasma depend only on the coordinate z , the accretion rate can

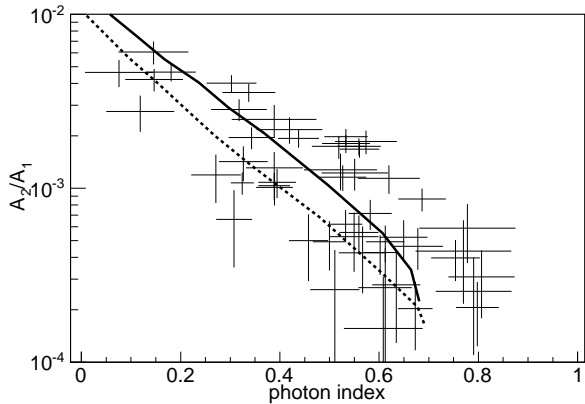


FIG. 5.— Relation between A_2/A_1 and the photon index Γ of the negative power-law component extracted from the *Suzaku* analysis of Vela X-1. Error bars indicate 1σ uncertainties. The simulation models for $kT = 6$ keV (solid) and $kT = 10$ keV (dashed) are also superposed.

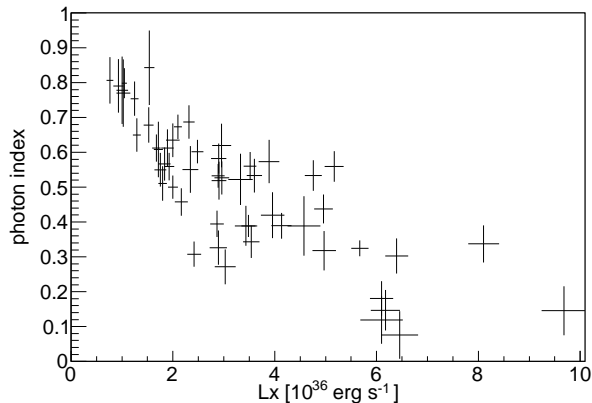


FIG. 6.— Relation between the photon index Γ and the X-ray luminosity. This plot is taken from Fig. 19 in Paper I.

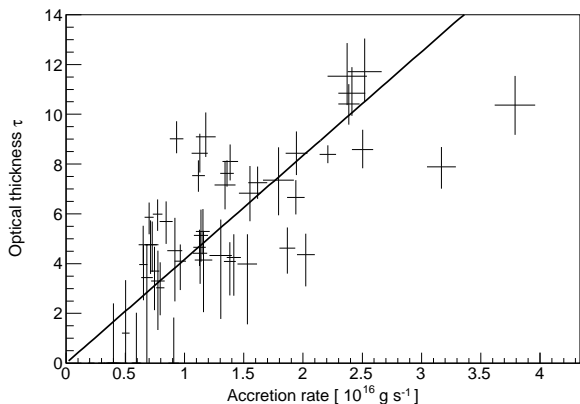


FIG. 7.— Relation between the effective optical thickness τ and the accretion rate \dot{M} . The solid line shows a linear function described by Equation (8).

be written as

$$\dot{M} = \pi r_0^2 n(z) m_p |v(z)|. \quad (9)$$

The optical thickness in the horizontal direction (r -direction) from the center to the wall surface is

$$\tau = r_0 n(z) \sigma_{\perp}. \quad (10)$$

Substituting Equations (9) and (10) to Equation (8), we obtain the column radius as

$$r_0 = \frac{\sigma_T}{\pi m_p} \frac{\dot{M}}{\tau v} = 1.0 \times 10^5 \left(\frac{0.1c}{v} \right) \text{ cm}. \quad (11)$$

Here, we assumed $\sigma_{\perp} = \sigma_T$. If the velocity of the decelerated accretion flow is $0.1c$ near the surface, the radius of the accretion column in Vela X-1 is ~ 1 km. This value is natural by comparison with the neutron star radius $R_* \sim 10$ km, which reinforces the hypothesis of the emission mechanism due to Comptonization.

4.1. Simulation of Accretion Column

Based on the dynamical structure described above, we performed Monte Carlo simulations of Comptonized X-ray radiations. The calculation methods are given in Appendix §A. The geometry including the distributions of the number density and the velocity is completely specified by three parameters: the mass accretion rate \dot{M} , the column radius r_0 , and the height of the sonic point z_{sp} . The accretion rate is determined by the luminosity L_X if the mass $M_* = 1.9M_{\odot}$ (Quaintrell et al. 2003), and radius $R_* = 10^6$ cm of the neutron star are fixed. The sonic point z_{sp} is represented as $z_{\text{sp}} = \xi r_0$, where we introduce a dimensionless scaling parameter ξ . Equation 5 shows that according to the analytical solution obtained by Basko & Sunyaev (1976) and Becker (1998), the value of this parameter should depend on the ratio of the energy-averaged cross sections that determine interaction rates for photons propagating parallel and perpendicular to the magnetic field, and is expected to be almost constant **if the energy spectrum of the radiation does not largely change.**

According to the velocity profile (Equation 4), the velocity reaches zero at the surface of neutron star, and therefore the number density becomes very large. It implies the existence of a “photosphere”, i.e. a height below which the density is sufficiently large to be optically thick. Since photon absorption occurs via free-free absorption in this regime, the position of the photosphere can be estimated as a point at which horizontal optical thickness of free-free absorption becomes unity (Becker & Wolff 2007). This relation is represented as

$$\alpha_R^{\text{ff}} r_0 = 1 \quad (12)$$

where α_R^{ff} denotes the Rosseland-mean of free-free absorption coefficient, and can be represented in cgs units as (Rybicki & Lightman 1979)

$$\alpha_R^{\text{ff}} = 1.7 \times 10^{-25} T^{-7/2} n^2 \text{ cm}^{-1}. \quad (13)$$

We regard the position z_b given by this relation as the bottom of the accretion column, and this surface at $z = z_b$ can be treated as a blackbody emitter.

We have used the Monte Carlo approach to calculate the spectrum of the photons escaping from the accretion

column, based on the source function of seed photons (see Appendix A of Odaka et al. 2011, for the description of the numerical approach). In the accretion column the seed photons are provided by thermal bremsstrahlung from the plasma, cyclotron radiation of electrons in the strong magnetic field, and blackbody radiation from the bottom of the column. In this paper we compute only the Comptonization of the thermal bremsstrahlung photons, other contributions will be considered elsewhere. However, we note that in the case of **high luminosity** sources, bremsstrahlung provides the dominant donor of seed photons among the three processes (Becker & Wolff 2007).

For thermal bremsstrahlung, the source function, or a photon production rate, is given by Equation (6). As the emissivity is proportional to the density squared, n^2 , the seed photons concentrate near the bottom of the column, where the density is large due to the deceleration of the accretion flow. For the sake of simplicity, we assume that the seed photons are isotropic, though the strong magnetic field can significantly affect the direction distribution of the free-free emission. A beaming effect due to the bulk motions is negligible since most of the seed photons come from the bottom region of the column, where the falling flow is sufficiently decelerated.

The simulation parameters are listed in Table 1. In these simulations, we assumed a column radius $r_0 = 4 \times 10^4$ cm; plasma temperature $kT = 6$ keV; and three values of $\xi = z_{\text{sp}}/r_0 = 0.5, 1.0, 2.0$. The spectra obtained by the simulations and fitted parameters of the NPEX model are shown in Figure 8 and Table 2, respectively. The spectral shape strongly depends on ξ because this parameter controls the density of the decelerated plasma. For $\xi = 2.0$, the spectrum is nearly saturated, being dominated by the Wien spectrum (for detail, see, e.g., Rybicki & Lightman 1979, §7.7). Note that for this case, the fitted values regarding the negative power-law term, i.e. Γ and A_1 , are no longer good indicators of the degree of Comptonization, since the fitted positive power-law term of the NPEX function completely dominates over the negative power-law term (see Table 2 and the right panel of Figure 8). In other words, characterization using the NPEX function fails in this regime.

TABLE 1
SIMULATION PARAMETERS OF THE ACCRETION COLUMN

| parameter | value |
|--------------------------------|------------------------------------|
| Luminosity L_X (0.1–100 keV) | 3.0×10^{36} erg s $^{-1}$ |
| Neutron star mass M_* | $1.9M_\odot$ |
| Neutron star radius R_* | 10^6 cm |
| Column radius r_0 | 4.0×10^4 cm |
| Electron temperature kT | 6 keV |
| $\xi = z_{\text{sp}}/r_0$ | 0.5, 1.0, 2.0 |

4.2. Magnetic Field Effects

The strong magnetic field of $B \sim 10^{12}$ G close to the neutron star surface largely affects the interactions between photons and electrons. Namely, in such a strong field, electrons are allowed to move only along the field lines, while the perpendicular motion is quantized to

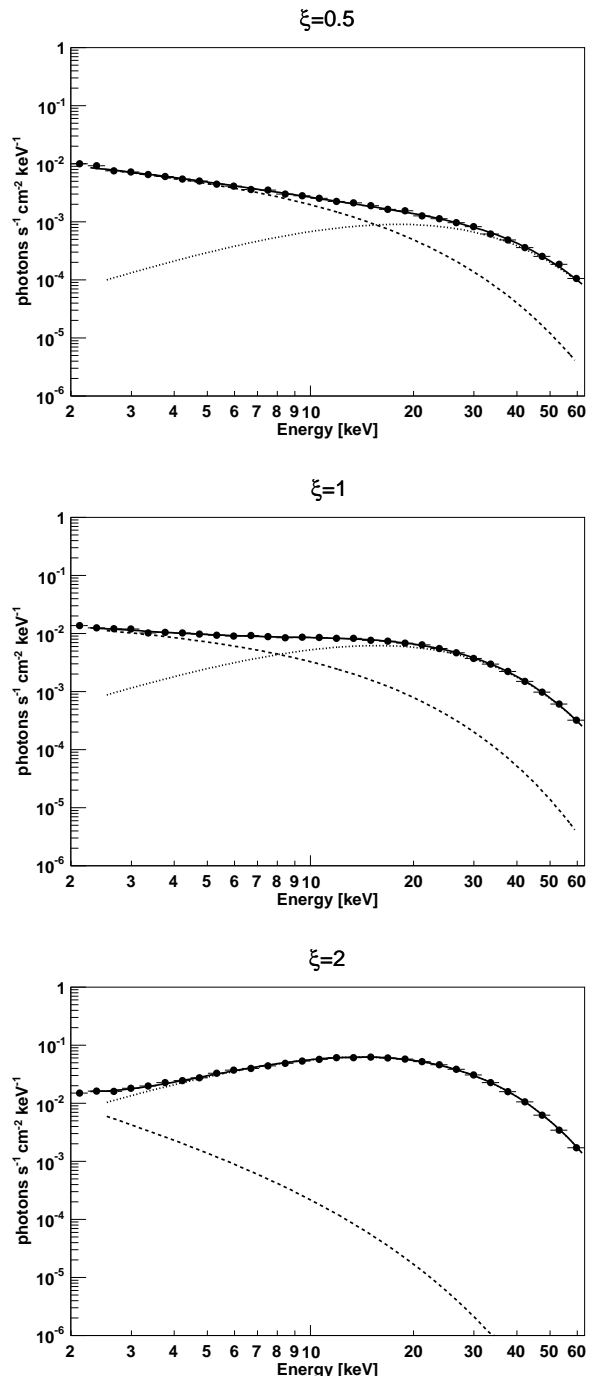


FIG. 8.— Simulation spectra of thermal and bulk Comptonization from the accretion column. The simulation parameters are tabulated at the top of each panel. The value of the $\xi = z_{\text{sp}}/r_0$ is indicated at the top of each panel. Fitted NPEX model (solid), the negative (dashed) and the positive (dotted) power-law components are superposed. The model parameters obtained by the fit are tabulated in Table 2. Statistical errors due to Monte Carlo sampling are sufficiently small compared with the filled circles showing the simulation data points.

Landau states. The imposed kinematic restrictions imply a significant change of the interaction cross-section, which gets reduced, particularly for photons that propagate parallel to the field. In addition, transitions between discrete energy levels corresponding to the “perpendicular” motion of electrons (Landau levels), results in forma-

TABLE 2
FITTED VALUES OF THE SIMULATED SPECTRA TO THE NPEX MODEL

| ξ | L_0 erg s ⁻¹ | A_1 ph s ⁻¹ cm ⁻² keV ⁻¹ | Γ | A_2 ph s ⁻¹ cm ⁻² keV ⁻¹ | E_f keV | L_X erg s ⁻¹ | A_2/A_1 |
|------------------|------------------------------|--|----------|--|--------------|------------------------------|----------------------|
| 0.5 | 8.77×10^{35} | 1.5×10^{-2} | 0.41 | 2.1×10^{-5} | 9.0 | 8.9×10^{35} | 1.4×10^{-3} |
| 1.0 | 2.39×10^{36} | 1.9×10^{-2} | 0.20 | 1.9×10^{-4} | 7.8 | 3.4×10^{36} | 1.0×10^{-2} |
| 2.0 ^a | 4.44×10^{36} | 4.0×10^{-2} | 1.65 | 2.3×10^{-3} | 7.1 | 2.4×10^{37} | 5.8×10^{-2} |

a) For this case, the characterization by the NPEX function fails. (See text in detail.)

tion of the so-called cyclotron emission and absorption.

Although the physical processes of photons in a strong magnetic field are very complex (e.g. Ventura 1979; Kirk & Meszaros 1980; Arons et al. 1987), we rely here on a simple treatment of the photon propagation in the magnetic field, which is based on our Comptonization model described in Appendix §A. Since the reduction of the scattering cross sections is the most significant effect of the magnetic field on the photon propagation, the total cross sections for photon interactions are modified in our treatment. Such a strong magnetic field leads to a birefringent nature of the photon propagation. Thus, we distinguish scattering of two linearly polarized normal modes, ordinary and extraordinary. The ordinary mode is linearly polarized with electric field vector that is placed in the plane formed by the photon propagation direction and the magnetic field; while the extraordinary mode has electric field vector perpendicular to this plane. Approximate total cross sections of the ordinary (1) and extraordinary (2) mode are given by

$$\sigma^{(1)}(E) = \sigma_T[\sin^2 \theta + f(E) \cos^2 \theta], \quad (14)$$

$$\sigma^{(2)}(E) = \sigma_T f(E), \quad (15)$$

respectively, where σ_T is the Thomson cross section, θ is the angle between the photon direction and the magnetic field, and the $f(E)$ is given by

$$f(E) = \begin{cases} \left(\frac{E}{E_c}\right)^2 & (E \leq E_c) \\ 1 & (E \geq E_c) \end{cases}, \quad (16)$$

where E_c denotes the cyclotron energy (Arons et al. 1987). Since cyclotron resonance scattering is effective only near the resonance energy E_c , we do not include this process in the total cross section of the scattering, though the cross section of the resonance effect is significant at $E = E_c$.

Although, the presence of the magnetic field changes the electron distribution and differential cross sections of the scattering processes, the other parts of the calculation, which include the sampling of the target electron and the determination of the scattered photon in the rest frame of the target, remain unmodified for simplicity. Consequently, including the magnetic field in our model of Comptonization (Appendix §A) only affects the determination of the next interaction point in terms of the Monte Carlo simulations.

Simulation results based on this model are shown in Figure 9 and Table 3. The conditions of the accretion column are completely identical to the simulations demonstrated in the previous subsection (§4.1) except that these simulations account for the presence of mag-

netic field with $B = 2 \times 10^{12}$ G. All the three spectra qualitatively agree with spectral features of accreting X-ray pulsars, which are represented by the NPEX model. The effect of the reduced cross sections is obvious from the mildly Comptonized spectrum even for $\xi = 2.0$. Since Comptonization becomes significant with ξ , the photon index Γ and the normalization ratio A_2/A_1 increase with ξ .

5. DISCUSSION

Our radiation model of thermal and bulk Comptonization in an accretion column with a strong magnetic field well reproduces the broad-band spectral characteristics observed from accreting neutron stars. Based on the model, we find self-consistent solutions that agree well with the observed spectra of Vela X-1. We study solutions where the accretion plasma itself provides the seed photons through free-free emission. Thus, the simulation model has only three parameters: the X-ray luminosity L_{obs} obtained by observation, the radius of the accretion column r_0 , and the ratio of the the sonic-point height to the column radius $\xi = z_{\text{sp}}/r_0$. While r_0 and ξ determine the geometry of the column including the z -profiles of the velocity and the density, the observed luminosity L_{obs} determines the accretion rate \dot{M} , i.e. the normalization of the density distribution. Once these three parameters fix the simulation geometry, the distribution of the seed photons, i.e. the source function, is uniquely determined. The total luminosity L_0 of the seed photons thus obtained is also tabulated in Table 2 and 3. The simulation results also allow the luminosity L_X to be determined. Under the assumption that the accretion plasma itself is responsible for the X-ray emission and reprocessing via Compton scattering, the luminosity L_X obtained in the simulations has to agree with the observed luminosity L_{obs} , from which we constructed the simulation geometry, to keep self consistency of the model.

If this model were firmly established and the dependence on the parameters were well understood, spectral fitting of the simulation model to the observed spectra would be a powerful way to obtain the physical properties of the accretion column. Such analysis is, however, beyond the scope of this paper. Instead, we investigate the basic behavior of the numerical model for different values of the parameters. For example, the simulation results, presented in §4.2, show that for a fixed column radius r_0 the Comptonized radiation becomes harder and more luminous when ξ increases. Similarly, we have studied the spectral dependence on r_0 with a fixed value of $\xi = 1.5$. The modeling data summarized in Table 4 show that the photon index Γ becomes softer with increase of r_0 . Obviously, this softening is related to the decrease

TABLE 3
FITTED VALUES OF THE SIMULATED SPECTRA WITH A MAGNETIC FIELD TO THE NPEX MODEL

| ξ | L_0 erg s $^{-1}$ | A_1 ph s $^{-1}$ cm $^{-2}$ keV $^{-1}$ | Γ | A_2 ph s $^{-1}$ cm $^{-2}$ keV $^{-1}$ | E_f keV | L_X erg s $^{-1}$ | A_2/A_1 |
|-------|------------------------|--|----------|--|--------------|------------------------|----------------------|
| 0.5 | 8.77×10^{35} | 1.0×10^{-1} | 1.05 | 3.1×10^{-5} | 7.8 | 9.7×10^{35} | 3.1×10^{-4} |
| 1.0 | 2.39×10^{36} | 2.4×10^{-1} | 0.85 | 1.8×10^{-4} | 7.0 | 3.2×10^{36} | 7.5×10^{-4} |
| 2.0 | 4.44×10^{36} | 3.1×10^{-1} | 0.51 | 6.1×10^{-4} | 6.6 | 7.8×10^{36} | 2.0×10^{-3} |

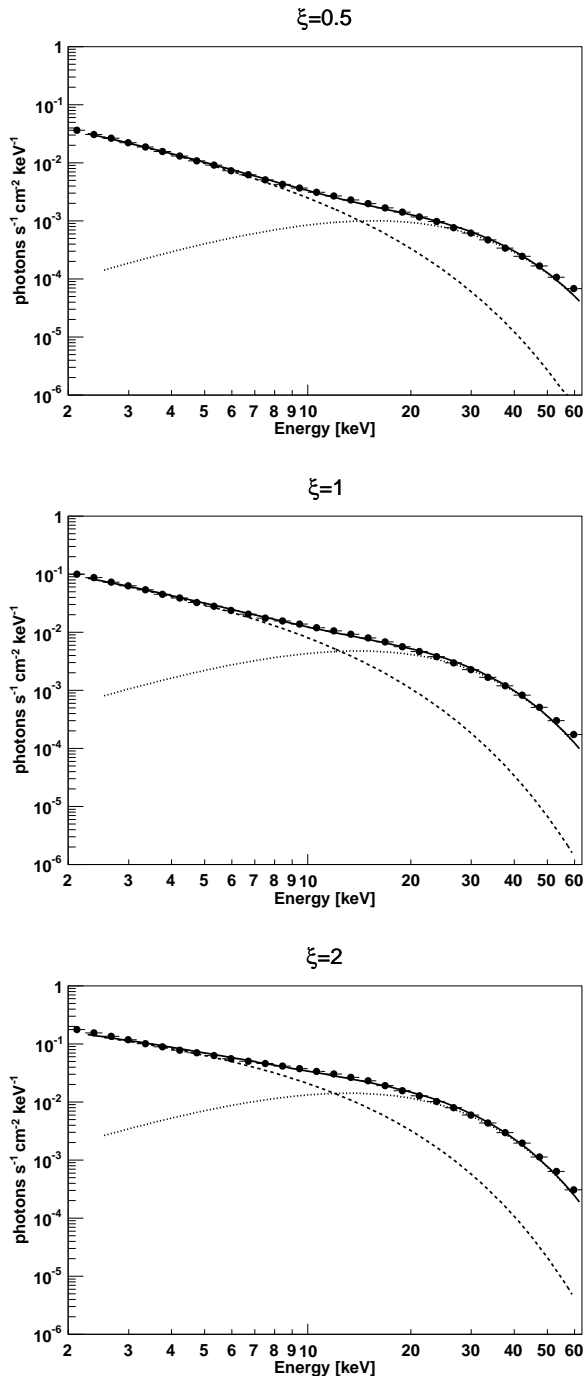


FIG. 9.— Same as Figure 8 but for accretion columns that have a strong magnetic field of $B = 2 \times 10^{12}$ G. The model parameters obtained by the fit are tabulated in Table 3.

of the optical depth across the column, which is approximately proportional to r_0^{-1} . The dependence of L_X on r_0 is more complex. On the one hand, the luminosity L_0 of the seed photons, which are produced via free-free emissions, increases with r_0 ; however, the energy gain by the Comptonization becomes effective for small r_0 , i.e. for large optical thickness. Thus, the dependence of luminosity L_X on r_0 is determined by the competition of these two effects. The data, presented in Table 4, show that the luminosity barely depends on the column radius for the considered range of parameters.

The inferred dependencies on the model parameters allowed us to find acceptable self-consistent solutions for the observed luminosities, which range from 1.5×10^{36} erg s $^{-1}$ to 6×10^{36} erg s $^{-1}$. The obtained parameters are tabulated in Table 5, we note that all acceptable solutions correspond to the unique value of ξ parameter, $\xi = 1.25$. This value is consistent with a rough estimate by Equation 5 for typical photon energy of ~ 5 keV, which should be close to the thermal energy. The cross sections for the different (perpendicular and parallel) directions can be written as $\sigma_{\perp} \simeq \sigma_T$ and $\sigma_{\parallel} \simeq (\bar{E}/E_c)^2 \sigma_T$ (See Equations 6 and 7 of Becker & Wolff (2007)). As can be seen in Table 5, the solutions satisfy the self-consistent condition $L_{\text{obs}} \sim L_X$ and have reasonable values of the column radius. These solution reproduce the observed spectral hardening with increase of the luminosity, and interestingly suggest a positive correlation between the column radius and mass accretion rate. However, at the present stage we cannot exclude presence of other possible solutions.

Finally, we can interpret the spectral shape typical for a “low state” into which Vela X-1 sometimes drops. Since the source still shows X-ray pulsations during the low states, it is evident that the accretion flow still reaches the magnetic poles of the neutron star. In the low state, the accretion rate is an order of magnitude lower than that of the normal state, though the physical mechanism of the suppression is unknown. The extremely soft power law with photon index of ~ 2 is difficult to explain by thermal mechanism including the thermal Comptonization, as shown in Figure 3. Bulk Comptonization, however, naturally features such a soft spectrum. We therefore suggest that the bulk Comptonization dominates over the thermal processes in the low state of the accreting neutron star.

6. CONCLUSIONS

We studied the process of Comptonization in the accretion column of binary pulsars. Our calculations were based on a Monte Carlo framework MONACO and aimed to explain the data obtained with the *Suzaku* X-ray observatory from brightest wind-fed accreting neutron star Vela X-1. The observational data used were reported in

TABLE 4
FITTED VALUES OF THE SIMULATED SPECTRA FOR DIFFERENT COLUMN RADII

| r_0 m | L_0 erg s $^{-1}$ | A_1 ph s $^{-1}$ cm $^{-2}$ keV $^{-1}$ | Γ | A_2 ph s $^{-1}$ cm $^{-2}$ keV $^{-1}$ | E_f keV | L_X erg s $^{-1}$ | A_2/A_1 |
|------------|------------------------|--|----------|--|--------------|------------------------|----------------------|
| 200 | 2.26×10^{36} | 5.6×10^{-2} | 0.15 | 3.0×10^{-4} | 6.7 | 3.8×10^{36} | 5.4×10^{-3} |
| 300 | 3.05×10^{36} | 1.2×10^{-1} | 0.45 | 3.4×10^{-4} | 6.6 | 4.0×10^{36} | 2.8×10^{-3} |
| 400 | 3.67×10^{36} | 1.9×10^{-1} | 0.58 | 2.5×10^{-4} | 6.9 | 4.0×10^{36} | 1.3×10^{-3} |

TABLE 5
THE SELF-CONSISTENT SOLUTIONS OF THE ACCRETION COLUMN SPECTRUM

| L_{obs} erg s $^{-1}$ | r_0 m | L_0 erg s $^{-1}$ | A_1 ph s $^{-1}$ cm $^{-2}$ keV $^{-1}$ | Γ | A_2 ph s $^{-1}$ cm $^{-2}$ keV $^{-1}$ | E_f keV | L_X erg s $^{-1}$ | A_2/A_1 |
|-----------------------------------|------------|------------------------|--|----------|--|--------------|------------------------|----------------------|
| 1.5×10^{36} | 150 | 9.19×10^{35} | 3.4×10^{-2} | 0.58 | 0.0 | 17 | 1.2×10^{36} | 0 |
| 3.0×10^{36} | 150 | 1.68×10^{36} | 5.3×10^{-1} | 0.34 | 2.9×10^{-4} | 6.6 | 3.0×10^{36} | 5.5×10^{-4} |
| 4.5×10^{36} | 200 | 2.37×10^{36} | 5.5×10^{-1} | 0.17 | 4.4×10^{-4} | 6.6 | 4.4×10^{36} | 8.0×10^{-4} |
| 6.0×10^{36} | 300 | 3.51×10^{36} | 6.7×10^{-1} | 0.03 | 4.4×10^{-4} | 6.9 | 6.2×10^{36} | 6.6×10^{-4} |

Paper I, where a long exposure (100 ks) was split into 56 short timescale (2 ks) spectra to study the variability. These X-ray spectra are best fitted by the NPEX model, which is a combination of two different-slope power laws with a common exponential cutoff, with an obvious cyclotron resonance scattering feature at 50 keV (Paper I).

Our study has shown that NPEX-type spectra are consistent with a Comptonization origin. This association allows us to link phenomenological parameters in the NPEX model with the physical properties of the production site of the X-ray emission. In particular, we show that the photon index Γ can be used as a good measure of the source optical depth. This therefore suggests a physical interpretation for an observed correlation between the photon index Γ and X-ray luminosity: the optical thickness of the accreted plasma increases with the mass accretion rate onto the neutron star.

A more detailed study of a magnetized accretion column showed that the broad-band X-ray spectra obtained with *Suzaku* can be well explained as Comptonized emission produced in the accretion column with a strong magnetic field of $\sim 10^{12}$ G. Importantly, within this interpretation, the *Suzaku* spectra are consistent with physically reasonable values of the parameters describing the geometry of the accretion column.

Finally, we find that thermal Comptonization is unlikely to be responsible for the soft spectra (with a photon index of ~ 2) measured during “low states”, in which the source luminosity becomes an order of magnitude lower than that of the normal state. Since these states still shows X-ray pulsations, indicating that the accretion flow reaches to the magnetic poles on the neutron star (Paper I), we suggest that such a soft power law is most likely produced via Comptonization dominated by the bulk motion rather than thermal processes.

part by Global COE Program (Global Center of Excellence for Physical Sciences Frontier), MEXT, Japan.

The authors are grateful to Prof. Chris Done for her useful comments on the manuscript. H. Odaka and Y. Tanaka had been supported by research fellowships of the Japan Society for the Promotion of Science for Young Scientists. This work was supported by JSPS KAKENHI Grant Number 24740190. This work was supported in

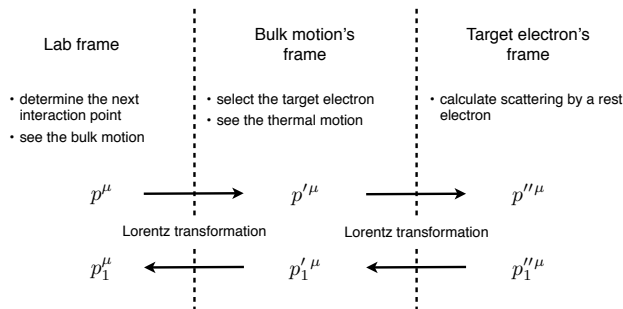


FIG. 10.— Schematic outline of calculation for inverse Compton scattering. p^μ and p_1^μ denote energy-momentum vectors of an incident and scattered photon, respectively. (μ is a coordinate index that runs from 0 to 3.)

APPENDIX

CALCULATION OF THERMAL AND BULK COMPTONIZATION

Comptonization is one of the main processes for production of X-ray radiations in accretion flows. In this process a photon is up-scattered to higher energy by a high-energy electron. Depending on energy distribution of the electrons, the dominant contribution to the Comptonization can be related either to thermal or bulk motion of the electrons. Therefore, one distinguishes *thermal* and *bulk* Comptonization processes. In compact binary systems, both of these processes typically lead to formation of spectra peaking in the X-ray energy band. Indeed, in the case of thermal Comptonization, the energy of up-scattered photons saturates close to the electron temperature. Similarly, free fall velocity, which serves as a good measure of the bulk velocity, onto a neutron star achieves $0.5c$. Thus, bulk Comptonization is also expected to peak in the X-ray band.

Many important features of the Comptonization have been obtained with an analytical approach. In particular, Kompaneets Equation proved to be very useful for studying thermal Comptonization (e.g., Rybicki & Lightman 1979; Sunyaev & Titarchuk 1980; Titarchuk 1994). However, the analytical approaches have several limitations (see, e.g., Hua 1997). For example, the photon transport equation typically implies that the energy and position of photons are continuous functions of time. This assumption is a good approximation for low energy bands since scattering at low energy does not change the photon energy significantly. At higher energies, this assumption breaks due to a substantial change of the photon energy in a single scattering. The analytical methods are also not suitable for a precise description of the photon escape, which is strongly affected by the geometrical structure of the production region. By contrast, it is possible to address all these limitations in Monte-Carlo-type simulations, where both detailed photon transport and precise scattering process are automatically accounted for. While Monte Carlo simulations have been performed by a few groups (see, e.g., Pozdnyakov et al. 1983; Hua 1997) for thermal Comptonization, we exploit an approach which includes both thermal and bulk Comptonization in complicated geometries.

We build our numerical procedure on a sequence of computations performed in different coordinate systems with the physical quantities being related via corresponding Lorentz transformations. We use three coordinate systems: *laboratory* (i.e., the observer system), *bulk* (where electron's bulk velocity is zero) and *electron rest* frames. A sketch of the implementation is shown in figure 10. The laboratory frame is used to compute the photon path, and the electron rest frame is suitable for detailed calculations of the scattering.

The mean interaction rate for a photon in the laboratory frame can be obtained by averaging the number of scattering (ν) per unit of time ($ds = cdt$) over the electron distribution:

$$\left\langle \frac{d\nu}{ds} \right\rangle = \int dE_e \int d\Omega_e (1 - \beta \cos \theta) \sigma(E') N_e(E_e, \Omega_e), \quad (\text{A1})$$

where $\beta = v_e/c$ is an electron velocity; θ is the angle between the electron and photon velocities; $N_e(E_e, \Omega_e) = dN/(dV dE_e d\Omega_e)$ is the electron distribution function for energy E_e and direction Ω_e ; $\sigma(E')$ is the invariant scattering cross section computed in the electron rest frame (for detail see, e.g., Landau & Lifshitz 1979). Since the physical region of interest here has an X-ray energy $E \lesssim 100$ keV and a low electron temperature $kT \lesssim 10$ keV, the cross section has weak energy dependence, and the thermal motion of the electrons is negligible in the calculation of the mean free path. Thus, Equation A1 can be simplified as

$$\left\langle \frac{d\nu}{ds} \right\rangle \approx (1 - \beta_b \cos \theta) \sigma(E') n_e. \quad (\text{A2})$$

Here, $\beta_b = v_b/c$ is the bulk velocity; θ is the angle between the bulk motion and the incident photon direction; E' is the Doppler shifted energy of the incident photon in the bulk motion reference frame. Consequently, the mean free path of photons is given by

$$l \approx \frac{1}{(1 - \beta_b \cos \theta) \sigma(E') n_e}. \quad (\text{A3})$$

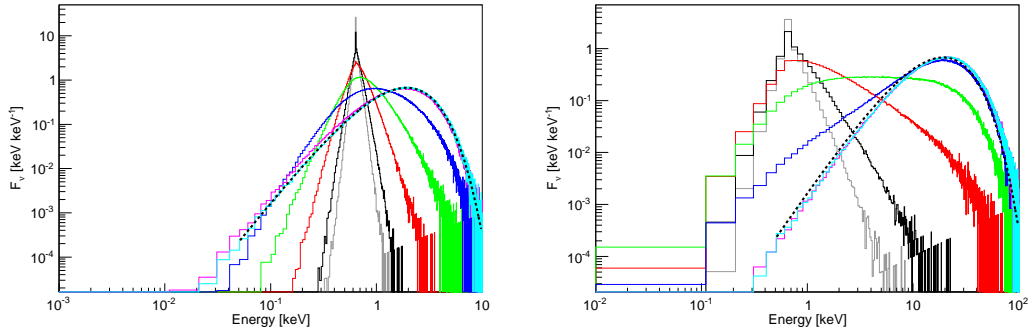


FIG. 11.— Right: energy spectra F_ν of Comptonized radiations from a spherical plasma with a temperature of $kT = 0.64$ keV for different radial optical (Thomson) depths $\tau = 1$ (grey), 2 (black), 5 (red), 10 (green), 20 (blue), 50 (magenta), and 100 (cyan). The source photon is generated at the center and $E_0 = 0.64$ keV. The Wien spectrum at the same temperature is superposed as the dashed curve. Left: the same as the right panel but for an electron temperature of $kT = 6.4$ keV.

Once the Monte Carlo code samples the interaction point based on the photon direction and the value of the mean free path l , the scattering process is computed. The numerical procedure for calculation of the photon-electron interaction consists of two steps: first, the scattering electron is selected via evaluation in the bulk reference frame; second, the final state of the scattered photon is computed in the electron rest frame. Using Equation (A1) in the bulk reference frame, we can evaluate the interaction probability as

$$P(E'_e, \Omega'_e) \propto (1 - \beta' \cos \theta') \sigma(E'') N_e(E'_e). \quad (\text{A4})$$

Here, prime indicates values in the reference frame of the bulk motion, not the laboratory frame; double prime indicates values in the electron rest frame. Since the energy dependence of the cross section is negligible for low temperature ($kT \lesssim 10$ keV) plasma, the direction and energy of the electron can be sampled independently. Namely, the electron velocity $v' = \beta'/c = \sqrt{2E'_e/m_e}$ is sampled from the Maxwell distribution

$$N_e(v) dv = \sqrt{\frac{2}{\pi}} \left(\frac{m_e}{kT}\right)^3 v^2 \exp\left(-\frac{m_e v^2}{2kT}\right) dv; \quad (\text{A5})$$

and the direction of the electron motion β' obtained from

$$P(\cos \theta') \propto 1 - \beta' \cos \theta'. \quad (\text{A6})$$

The numerical procedure outlined above allows us to obtain energy E''_1 and direction Ω''_1 of the scattered photon in the electron rest frame by using the Klein-Nishina differential cross section. Finally, we use a reverse Lorentz transformation in order to obtain the result of the Compton scattering seen by the observer.

In order to verify our simulation code, we calculated thermal Comptonization radiation (the bulk velocity was assumed to be zero) from a spherically symmetric cloud of fully ionized plasma. This is the simplest model to check X-ray spectra generated by Comptonization. We have performed calculations for two different electron temperatures of $kT = 0.64$ keV and 6.4 keV.

The initial photons start at the center of the cloud $\mathbf{x}_0 = (0, 0, 0)$ with an initial energy 0.64 keV. The left panel of Figure 11 shows the results for different radial optical (Thomson) depths ranging from $\tau = 1$ to 100 and for the common temperature $kT = 0.64$ keV. For $\tau = 1$, the spectrum is not largely altered from the initial spectrum because the escaped photons have experienced zero or a few scatterings by electrons. As the optical depth increases, the photon spectrum “evolves” to the saturated Comptonization or thermal equilibrium. The spectrum for $\tau = 100$, which is a result of ~ 10000 interactions with electrons, nicely agrees with the Wien spectrum at $kT = 0.64$ keV, as predicted theoretically.

The right panel of Figure 11 shows the same calculation except for the electron temperature $kT = 6.4$ keV, i.e., ten times higher than the first example. The initial conditions or source photons are the same for both the models. The photons undergo faster heating due to the higher electron temperature. There is a broad peak at $E \simeq 3kT \sim 20$ keV, the “Wien hump” generated by the saturated Comptonization for a large optical depth, whereas the unsaturated emission from $\tau = 1$ forms a power-law-like spectrum. The spectral index of the power-law component strongly depends on the optical depth of the Comptonizing cloud.

REFERENCES

- Arons, J., Klein, R. I., & Lea, S. M. 1987, *ApJ*, 312, 666
 Basko, M. M., & Sunyaev, R. A. 1976, *Royal Astronomical Society*, 175, 395
 Becker, P. 1998, *ApJ*, 498, 790
 Becker, P. A., & Wolff, M. T. 2005, *ApJ*, 621, L45
 —. 2007, *ApJ*, 654, 435
 Bondi, H., & Hoyle, F. 1944, *MNRAS*, 104, 273
 Frank, J., King, A., & Raine, D. 2002, *Accretion Power in Astrophysics* (Cambridge University Press)
 Hua, X.-M. 1997, arXiv, physics.comp-ph
 Kirk, J. G., & Meszaros, P. 1980, *ApJ*, 241, 1153
 Kokubun, M., et al. 2007, *PASJ*, 59, 53

- Kreykenbohm, I., et al. 2008, *A&A*, 492, 511
- Landau, & Lifshitz. 1979, *Classical Theory of Fields*
- Makishima, K., Mihara, T., Nagase, F., & Tanaka, Y. 1999, *ApJ*, 525, 978
- Mihara, T. 1995, PhD thesis, University of Tokyo
- Mitsuda, K., et al. 2007, *PASJ*, 59, 1
- Odaka, H., Aharonian, F., Watanabe, S., Tanaka, Y., Khangulyan, D., & Takahashi, T. 2011, *ApJ*, 740, 1030
- Odaka, H., Khangulyan, D., Tanaka, Y. T., Watanabe, S., Takahashi, T., & Makishima, K. 2013, *ApJ*, 767, 70
- Pozdnyakov, L. A., Sobol, I. M., & Syunyaev, R. A. 1983, *Soviet Scientific Reviews*, 2, 189
- Quaintrell, H., Norton, A. J., Ash, T. D. C., Roche, P., Willems, B., Bedding, T. R., Baldry, I. K., & Fender, R. P. 2003, *A&A*, 401, 313
- Rybicki, G. B., & Lightman, A. P. 1979, *Radiative Processes in Astrophysics* (WILEY-VCH)
- Sunyaev, R. A., & Titarchuk, L. G. 1980, *A&A*, 86, 121
- Takahashi, T., et al. 2007, *PASJ*, 59, 35
- Titarchuk, L. 1994, *ApJ*, 434, 570
- Ventura, J. 1979, *Physical Review D - Particles and Fields*, 19, 1684
- Watanabe, S., et al. 2006, *ApJ*, 651, 421
- White, N. E., Swank, J. H., & Holt, S. S. 1983, *ApJ*, 270, 711